

November 13, 2018
hep-ph/01xxx

Complete next-to-leading order QCD corrections to charged Higgs boson associated production with top quark at the CERN Large Hadron Collider

SHOU-HUA ZHU

*Institut für Theoretische Physik, Universität Karlsruhe,
D-76128 Karlsruhe, Germany*

The complete next-to-leading order (NLO) QCD corrections to charged Higgs boson associated production with top quark through $bg \rightarrow tH^-$ at the CERN Large Hadron Collider are calculated in the minimal supersymmetric standard model (MSSM) and two-Higgs-doublet model in the \overline{MS} scheme. The NLO QCD corrections can reduce the scale dependence of the leading order (LO) cross section. The K-factor (defined as the ratio of the NLO cross section to the LO one) varies from ~ 1.4 to ~ 1.8 when charged Higgs mass and $\tan\beta$ are $180 \sim 1000$ GeV and $2 \sim 50$ respectively.

I. INTRODUCTION

The detection of the Higgs particles is one of the most important objectives of the Large Hadron Collider (LHC). Charged Higgs bosons are predicted in extended versions of the Standard model (SM), like two-Higgs-doublet models (2HDM) and the Minimal Supersymmetric Standard Model (MSSM). Discovery of such an additional charged Higgs boson will immediately indicate physics beyond the SM, unlike the case of the neutral Higgs boson. Hence, there is strong theoretical and experimental motivation for exploring the mechanisms of the charged Higgs boson production.

The charged Higgs boson H^\pm could appear as the decay product of primarily produced top quarks if the mass of H^\pm is smaller than $m_t - m_b$. For heavier H^\pm , the direct H^\pm production mechanisms at hadron colliders have been extensively investigated. At the LHC, the primary charged Higgs boson production channel is $gb \rightarrow H^- t$ [1] *. The study [3,4] shows that this production mechanism can be used to explore the parameter space of MSSM for m_{H^\pm} up to 1 TeV and $\tan\beta$ down to at least ~ 3 , and potentially to ~ 1.5 . Therefore, it is necessary to calculate and implement also the loop contributions to $gb \rightarrow H^- t$ for more accurate theoretical predictions.

In literature, the contribution of the initial-gluon process $gg \rightarrow H^- t \bar{b}$, which is only part of the next-to-leading order (NLO) QCD corrections to $gb \rightarrow H^- t$, has been calculated [5]. The supersymmetric electroweak corrections arising from the quantum effects which are induced by potentially large Yukawa couplings from the Higgs sector and the chargino-top(bottom)-sbottom(stop) couplings, neutralino-top(bottom)-stop(sbottom) couplings and charged Higgs-stop-sbottom couplings are also studied [1,6], which can give rise to a 15% reduction of the lowest-order result. In Ref. [7], the electro-weak corrections to the process are also discussed. In this paper, we deal with the complete NLO QCD corrections to $gb \rightarrow H^- t$.

The arrangement of this paper is as follows. Section II contains the analytic results, and in Section III we present numerical examples and discuss the implications of our results.

* See Ref. [2] for the discussion on other charged Higgs boson production mechanisms.

The lengthy expressions of the form factors are collected in the Appendix.

II. ANALYTIC EXPRESSIONS

Including the NLO QCD corrections, the cross sections for $PP \rightarrow tH^-X$ at the CERN LHC can be written as

$$\sigma = \sigma^{LO} + \sigma^{Vir} + \sigma^{Real}, \quad (1)$$

where σ^{LO} is the cross section at leading order (LO), σ^{Vir} and σ^{Real} are cross sections from NLO QCD corrections arising from virtual and real processes.

A. LO cross section

The Feynman diagrams for the charged Higgs boson production via $b(p_1)g(p_2) \rightarrow t(k_1)H^-(k_2)$ at the LO are shown in Fig.1. The amplitudes are created by use of Feynarts [8] and are handled with the help of FeynCalc [9]. As usual, we define the Mandelstam variables as

$$\begin{aligned} s &= (p_1 + p_2)^2 = (k_1 + k_2)^2, \\ t &= (p_1 - k_1)^2 = (p_2 - k_2)^2, \\ u &= (p_1 - k_2)^2 = (p_2 - k_1)^2. \end{aligned} \quad (2)$$

The amplitude at the LO could be written as

$$M_{LO} = \sum_{i=1}^6 t_i [c_1 M_{2i-1} + c_2 M_{2i}], \quad (3)$$

where the non-vanishing form factors are

$$\begin{aligned} t_2 &= \frac{1}{m_t^2 - u} - \frac{1}{s}, \\ t_3 &= \frac{2}{m_t^2 - u}, \\ t_5 &= -\frac{2}{s}, \end{aligned} \quad (4)$$

where $c_1 = \frac{g_w g_s \mu^{2\epsilon} m_b \tan \beta}{2\sqrt{2} m_w}$ and $c_2 = \frac{g_w g_s \mu^{2\epsilon} m_t \cot \beta}{2\sqrt{2} m_w}$. In Eq. (3) M_i is the standard matrix elements which are defined as

$$\begin{aligned}
M_1 &= \bar{u}(k_1) \not{e}(p_2) P_R u(p_1), \\
M_2 &= \bar{u}(k_1) \not{e}(p_2) P_L u(p_1), \\
M_3 &= \bar{u}(k_1) \not{p}_2 \not{e}(k_2) P_R u(p_1), \\
M_4 &= \bar{u}(k_1) \not{p}_2 \not{e}(k_2) P_L u(p_1), \\
M_5 &= \bar{u}(k_1) P_R u(p_1) k_1 \cdot \varepsilon(p_2), \\
M_6 &= \bar{u}(k_1) P_L u(p_1) k_1 \cdot \varepsilon(p_2), \\
M_7 &= \bar{u}(k_1) \not{p}_2 P_R u(p_1) k_1 \cdot \varepsilon(p_2), \\
M_8 &= \bar{u}(k_1) \not{p}_2 P_L u(p_1) k_1 \cdot \varepsilon(p_2), \\
M_9 &= \bar{u}(k_1) P_R u(p_1) p_1 \cdot \varepsilon(p_2), \\
M_{10} &= \bar{u}(k_1) P_L u(p_1) p_1 \cdot \varepsilon(p_2), \\
M_{11} &= \bar{u}(k_1) \not{p}_2 P_R u(p_1) p_1 \cdot \varepsilon(p_2), \\
M_{12} &= \bar{u}(k_1) \not{p}_2 P_L u(p_1) p_1 \cdot \varepsilon(p_2),
\end{aligned} \tag{5}$$

where the color matrix T^a has been suppressed. In this paper, we perform the calculations in Feynman gauge and in d time-space dimensions with $d = 4 - 2\epsilon$. For simplicity, we omit the bottom quark dynamical mass but keep the mass-term in Yukawa couplings.

The LO cross section can then be written as

$$\frac{d\sigma_{LO}}{dx_1 dx_2} = d\hat{\sigma}^0 G_{b/A}(x_1, \mu_f) G_{g/B}(x_2, \mu_f) + [A \leftrightarrow B], \tag{6}$$

with

$$d\hat{\sigma}^0 = \frac{1}{24} \frac{1}{4(1-\epsilon)} \frac{1}{2s} |M_{LO}|^2 d^N \Phi_2 \tag{7}$$

where the factor $\frac{1}{24}$ and $\frac{1}{4(1-\epsilon)}$ are the color and spin average, respectively, and two-body phase space is

$$d^N \Phi_2 = \frac{1}{8\pi} \left(\frac{4\pi}{s} \right)^\epsilon \frac{1}{\Gamma(1-\epsilon)} \left[\lambda \left(1, \frac{m_{H^\pm}^2}{s}, \frac{m_t^2}{s} \right) \right]^{1/2-\epsilon} v^{-\epsilon} (1-v)^{-\epsilon} dv, \tag{8}$$

with $v = \frac{1}{2}(1 + \cos \theta)$. Here λ is the two-body phase space function

$$\lambda(x, y, z) = x^2 + y^2 + z^2 - 2xy - 2xz - 2yz. \tag{9}$$

B. Virtual corrections

The Feynman diagrams for the NLO virtual corrections are shown in Fig. 2. The virtual diagrams which have the bubble on the external legs [conter-terms] are not shown. They can be obtained by inserting diagram (a)-(d) of Fig. 2 [conter-terms] into the external legs [external legs, internal propagators and vertex] of the LO diagrams in Fig. 1.

In order to remove the UV divergences, we have to renormalize the coupling constant and the quark mass. The strong coupling constant and the bottom quark mass are renomalized in the \overline{MS} scheme. However the top quark is renomalized in an on-shell scheme [10]. The useful renormalization constants are expressed as

$$\begin{aligned} \frac{\delta m_b}{m_b} &= -\frac{\alpha_s}{4\pi} 3C_F \Delta, \\ \frac{\delta m_t}{m_t} &= -\frac{\alpha_s}{4\pi} 3C_F \left[\Delta + \frac{4}{3} - \log(m_t^2/\mu^2) \right], \\ Z_b &= -\frac{\alpha_s}{4\pi} C_F \Delta, \\ Z_t &= -\frac{\alpha_s}{4\pi} C_F \left[\Delta - \log(m_t^2/\mu^2) \right], \\ Z_g &= -\frac{\alpha_s}{4\pi} \left[(2C_A - \beta_0)\Delta - \frac{2}{3} \log(m_t^2/\mu^2) \right], \\ \frac{\delta g_s}{g_s} &= -\frac{\alpha_s}{8\pi} \left[\beta_0 \Delta + \frac{2}{3} \log(m_t^2/\mu^2) \right] \end{aligned} \quad (10)$$

with $\Delta = \frac{1}{\epsilon} - \gamma_E + \log(4\pi)$, $\beta_0 = (11C_A - 2n_f)/3$, $C_A = 3$ and $C_F = 4/3$.

The renormalized virtual amplitude can then be written in the following way,

$$M_{\text{ren}} = M_A + M_B, \quad (11)$$

where M_A is the amplitude from the diagram (e)-(o) of Fig. 2 and M_B is the amplitude from the diagrams which contain bubble on the external legs or conter-terms.

The M_A can be written as

$$M_A = \sum_{i=e}^o M_A^i, \quad (12)$$

where i represents the diagram index of Fig. 2. For each diagram i , we can generally write the amplitude as

$$M_A^i = \sum_{j=1}^6 f_j [c_1 M_{2i-1} + c_2 M_{2i}], \quad (13)$$

where the non-vanishing form factor f_j are given explicitly in Appendix and the M_j is the standard matrix element given in the previous section.

The M_B can be written as

$$M_B = M_B^1 + M_B^2, \quad (14)$$

where

$$M_B^1 = M_{LO} \left\{ \frac{\delta g_s}{g_s} + \frac{Z_t}{2} + \frac{Z_b}{2} + \frac{Z_g}{2} + \frac{\alpha_s}{8\pi} \left[-3\Delta + \frac{8}{3} \log(m_t^2/\mu^2) - \frac{16}{3} \right] \right\}, \quad (15)$$

$$M_B^2 = \sum_{i=1}^6 [c_1 f_s^{2i-1} M_{2i-1} + c_2 f_s^{2i} M_{2i}]. \quad (16)$$

Here the non-vanishing form factors f_s^i ($i = 1 - 12$) are

$$\begin{aligned} f_s^1 &= f_s^2 = \frac{\delta m_t}{m_t^2 - u}, \\ f_s^3 &= \frac{-2m_t \delta m_t}{(m_t^2 - u)^2} + \frac{\delta m_b}{m_b} \left[\frac{1}{m_t^2 - u} - \frac{1}{s} \right], \\ f_s^4 &= \frac{-2m_t \delta m_t}{(m_t^2 - u)^2} + \frac{\delta m_t}{m_t} \left[\frac{1}{m_t^2 - u} - \frac{1}{s} \right], \\ f_s^5 &= 2 \left[\frac{-2m_t \delta m_t}{(m_t^2 - u)^2} + \frac{\delta m_b}{m_b} \frac{1}{m_t^2 - u} \right], \\ f_s^6 &= 2 \left[\frac{-2m_t \delta m_t}{(m_t^2 - u)^2} + \frac{\delta m_t}{m_t} \frac{1}{m_t^2 - u} \right], \\ f_s^9 &= -\frac{2}{s} \frac{\delta m_b}{m_b}, \\ f_s^{10} &= -\frac{2}{s} \frac{\delta m_t}{m_t}. \end{aligned} \quad (17)$$

After squaring the renormalized amplitude and performing the spin and color summations, the partonic cross section with virtual corrections can be written as

$$\frac{d\sigma^{Vir}}{dx_1 dx_2} = 2 \operatorname{Re} \left[\overline{\sum} (M_{\text{ren}}^+ M_{LO}) \right] d^N \Phi_2 G_{b/A}(x_1, \mu_f) G_{g/B}(x_2, \mu_f) + [A \leftrightarrow B]. \quad (18)$$

After the renormalization procedure described above, $d\sigma^{Vir}$ is UV-finite. Nevertheless, it contains still the infrared and collinear divergences. The infrared divergences will cancel against the contributions from soft-gluon radiation. The remaining collinear divergences will be removed by the redefinition of the parton distribution functions (PDF) (mass factorization).

C. Real corrections

There are three kinds of real corrections to the processes $bg \rightarrow tH^-$: gluon-radiation [$bg \rightarrow tH^-g$], initial-gluon [$gg \rightarrow tH^-\bar{b}$] and initial-active-quark [$bq(\bar{q}) \rightarrow tH^-q(\bar{q})$ and $q\bar{q} \rightarrow tH^-\bar{b}$, q stand for the active quarks which are treated as light for PDF evolution]. All real corrections are related to the $2 \rightarrow 3$ processes. In this paper, the $2 \rightarrow 3$ processes have been treated using the two cut-off phase space slicing method (TCPSSM) [11]. The method is briefly described in the following. Two small artificial constants δ_s , δ_c are introduced, and the three-body phase space can firstly be divided into soft and hard regions according to whether the gluon energy is less than $\delta_s\sqrt{s}/2$. Secondly the hard region is further divided into collinear and non-collinear regions according to whether the magnitude of $p_i \cdot p_j$ is less than $s/2$. In the soft and collinear regions, the phase space integration can be performed analytically in d-dimension. At the same time, in the non-collinear region, the phase space integration can be calculated in four dimension by standard Monte Carlo packages because the integration contains no divergences. Obviously, the final physical results should be independent on these artificial parameters δ_s and δ_c , which offers a crucial way to check our results. Therefore, the real corrections can be written as, according to the phase space slicing,

$$d\sigma^{Real} = d\sigma^S + d\sigma^{Coll} + d\sigma^{fin}, \quad (19)$$

where $d\sigma^S$, $d\sigma^{Coll}$ and $d\sigma^{fin}$ are cross sections in soft, collinear and non-collinear regions.

1. Cross section in soft region

The Feynman diagrams of the gluon-radiation process $bg \rightarrow tH^-g$ are shown in Fig. 3. They contribute to the cross section in the soft region. We may write the cross section as

$$\begin{aligned} \frac{d\sigma^S}{dx_1 dx_2} &= d\hat{\sigma}_S^0 G_{b/A}(x_1, \mu_f) G_{g/B}(x_2, \mu_f) + [A \leftrightarrow B], \\ d\hat{\sigma}_S^0 &= d\hat{\sigma}^0 \left[\frac{\alpha_s}{2\pi} \frac{\Gamma(1-\epsilon)}{\Gamma(1-2\epsilon)} \left(\frac{4\pi\mu_r^2}{s} \right)^\epsilon \right] \left(\frac{A_2^s}{\epsilon^2} + \frac{A_1^s}{\epsilon} + A_0^s \right), \end{aligned} \quad (20)$$

where

$$\begin{aligned}
A_2^s &= -\frac{4}{3} \frac{m_t^2 - t}{(E_1 - \beta \cos \theta)s} + 12 \frac{m_t^2 - u}{(E_1 + \beta \cos \theta)s} + 12, \\
A_1^s &= \frac{16}{3} \frac{4m_t^2}{(E_1^2 - \beta^2)s} + \frac{4}{3} \frac{m_t^2 - t}{(E_1 - \beta \cos \theta)s} (C_1 - 2 \log \frac{2}{\delta_s \sqrt{s}}) \\
&\quad + 12 \frac{m_t^2 - u}{(E_1 + \beta \cos \theta)s} (C_2 - 2 \log \frac{2}{\delta_s \sqrt{s}}) + 24 \log \frac{2}{\delta_s \sqrt{s}} - \log \frac{4}{s} A_2^s, \\
A_0^s &= \frac{1}{2} \log^2 \frac{4}{s} A_2^s - \log \frac{4}{s} A_1^s + \frac{16}{3} \frac{4m_t^2}{(E_1^2 - \beta^2)s} (2 \log \frac{2}{\delta_s \sqrt{s}} + \frac{E_1}{\beta} \log \frac{E_1 + \beta}{E_1 - \beta}) \\
&\quad + \frac{4}{3} \frac{m_t^2 - t}{(E_1 - \beta \cos \theta)s} (C_3 - 2 \log^2 \frac{2}{\delta_s \sqrt{s}} + 2C_1 \log \frac{2}{\delta_s \sqrt{s}}) \\
&\quad - 12 \frac{m_t^2 - u}{(E_1 + \beta \cos \theta)s} (C_4 - 2 \log^2 \frac{2}{\delta_s \sqrt{s}} + 2C_2 \log \frac{2}{\delta_s \sqrt{s}}) + 24 \log^2 \frac{2}{\delta_s \sqrt{s}}, \\
C_1 &= \log \frac{(E_1 - \beta \cos \theta)^2}{E_1^2 - \beta^2}, \\
C_2 &= \log \frac{(E_1 + \beta \cos \theta)^2}{E_1^2 - \beta^2}, \\
C_3 &= -\log^2 \frac{E_1 - \beta}{E_1 - \beta \cos \theta} + \frac{1}{2} \log^2 \frac{E_1 + \beta}{E_1 - \beta} - 2li_2(-\frac{-\beta \cos \theta + \beta}{E_1 - \beta}) + 2li_2(-\frac{\beta \cos \theta + \beta}{E_1 - \beta \cos \theta}), \\
C_4 &= -\log^2 \frac{E_1 - \beta}{E_1 + \beta \cos \theta} + \frac{1}{2} \log^2 \frac{E_1 + \beta}{E_1 - \beta} - 2li_2(-\frac{\beta \cos \theta + \beta}{E_1 - \beta}) + 2li_2(-\frac{-\beta \cos \theta + \beta}{E_1 + \beta \cos \theta}), \\
\beta &= \lambda^{\frac{1}{2}}(1, m_t^2/s, m_{H^\pm}^2/s), \\
E_1 &= \sqrt{\beta^2 + \frac{2m_t^2}{s}}. \tag{21}
\end{aligned}$$

2. Cross section in collinear region

In order to remove the collinear singularity, we should introduce a scale dependent parton distribution function (mass factorization). After factorization in $\overline{\text{MS}}$ convention, the cross section in collinear region can be written as

$$\begin{aligned}
\frac{d\sigma^{Coll}}{dx_1 dx_2} &= \left[\frac{\alpha_s}{2\pi} \frac{\Gamma(1-\epsilon)}{\Gamma(1-2\epsilon)} \left(\frac{4\pi\mu_r^2}{s} \right)^\epsilon \right] \left\{ G_{b/A}(x_1, \mu_f) G_{g/B}(x_2, \mu_f) \right. \\
&\quad \times \left[\frac{A_1^{sc}(b \rightarrow bg)}{\epsilon} + \frac{A_1^{sc}(g \rightarrow gg)}{\epsilon} + A_0^{sc}(b \rightarrow bg) + A_0^{sc}(g \rightarrow gg) \right] \\
&\quad + G_{b/A}(x_1, \mu_f) \tilde{G}_{g/B}(x_2, \mu_f) + \tilde{G}_{b/A}(x_1, \mu_f) G_{g/B}(x_2, \mu_f) \left. \right\} d\hat{\sigma}_0 \\
&\quad + [A \leftrightarrow B], \tag{22}
\end{aligned}$$

where [11]

$$A_0^{sc} = A_1^{sc} \ln \left(\frac{s}{u_f^2} \right) \quad (23)$$

$$A_1^{sc}(b \rightarrow bg) = C_F(2 \ln \delta_s + 3/2) \quad (24)$$

$$A_1^{sc}(g \rightarrow gg) = 2N \ln \delta_s + (11N - 2n_f)/6. \quad (25)$$

Here

$$\tilde{G}_{c/B,A}(x, \mu_f) = \sum_{c'} \int_x^{1-\delta_s \delta_{cc'}} \frac{dy}{y} G_{c'/B,A}(x/y, \mu_f) \tilde{P}_{cc'}(y) \quad (26)$$

with

$$\tilde{P}_{ij}(y) = P_{ij}(y) \ln \left(\delta_c \frac{1-y}{y} \frac{s}{\mu_f^2} \right) - P'_{ij}(y), \quad (27)$$

where

$$P_{qq}(z) = C_F \frac{1+z^2}{1-z} \quad (28)$$

$$P'_{qq}(z) = -C_F(1-z) \quad (29)$$

$$P_{gq}(z) = C_F \frac{1+(1-z)^2}{z} \quad (30)$$

$$P'_{gq}(z) = -C_F z \quad (31)$$

$$P_{gg}(z) = 2N \left[\frac{z}{1-z} + \frac{1-z}{z} + z(1-z) \right] \quad (32)$$

$$P'_{gg}(z) = 0 \quad (33)$$

$$P_{qg}(z) = \frac{1}{2} [z^2 + (1-z)^2] \quad (34)$$

$$P'_{qg}(z) = -z(1-z), \quad (35)$$

with $N = 3$.

3. Cross section in non-collinear region

As described above, the cross section in non-collinear region $d\sigma^{fin}$ can be easily obtained by Monte Carlo phase space integration in four dimension. It can be written as

$$\frac{d\sigma^{fin}}{dx_1 dx_2} = \sum_{q,q'} G_{q/A}(x_1, \mu_f) G_{q'/B}(x_2, \mu_f) |q q' \rightarrow t H^- X|^2 d\Phi_3 + [A \leftrightarrow B], \quad (36)$$

where q, q' run through gluon and light quarks and the three-body phase space Φ_3 is within the non-collinear region. In this paper, all Monte Carlo phase space integrations are performed by package BASES [12].

III. NUMERICAL RESULTS AND DISCUSSION

Our numerical results are obtained using CTEQ5M (CTEQ5L) PDF [13] and 2-loop (1-loop) evolution of $\alpha_s(\mu)$ for NLO (LO) cross section calculations with $\Lambda^{(5)} = 226$ (146) MeV. 2-loop evolution of the \overline{MS} bottom quark mass is adopted. The top-quark mass is taken to be $m_t = 175$ GeV; for simplicity, the renormalization and factorization scales are taken to be the same.

In Fig. 4 we show the K-factor, which is defined as

$$K = \frac{\sigma_{NLO}}{\sigma_{LO}}, \quad (37)$$

as a function of the charged Higgs mass with the renormalization and factorization scales $\mu = \mu_0$ ($\mu_0 = m_t + m_{H^\pm}$) and $\tan \beta = 50$. The different contributions to K-factor from Born (which is equal to 1 if the difference between the LO and NLO PDF and $\alpha_s(\mu)$ is omitted), virtual+gluon-radiation, initial-gluon, bq (\bar{q}) (q stand for the light quarks) and $q\bar{q}$ are also shown. From the figure, we can see that K-factor from Born contribution is around $1.1 \sim 1.2$. K-factor from virtual+gluon-radiation contribution is from 0.8 to 1 when the charged Higgs boson mass varies from 180 GeV to 1000 GeV. The initial-gluon and $bq(\bar{q})$ contributions to the K-factor are negative, and they vary from $\sim -26\%$ to $\sim -23\%$ and $\sim -5\%$ to $\sim -14\%$ respectively. The $q\bar{q}$ contribution to the K-factor can be neglected, the magnitude of which is smaller than 3% for all charged Higgs boson mass. Adding all the contributions, we can see that the K-factor varies from ~ 1.6 to ~ 1.8 when charged Higgs mass increases from 180 GeV to 1000 GeV.

In Fig. 5 we show the K-factor as a function of $\tan \beta$ for $m_{H^\pm} = 200, 500$ and 1000 GeV. It should be noted that the K-factor is independent on $\tan \beta$ if $\delta m_b/m_b = \delta m_t/m_t$ in Eq. (17). The K-factor increases with the increment of $\tan \beta$, and is insensitive to $\tan \beta$ when $\tan \beta \geq 20$.

In Fig. 6 we show the LO and NLO cross sections as a function of renormalization and factorization scales μ/μ_0 for $m_{H^\pm} = 200$ GeV and $\tan \beta = 50$. From the figure we can see that the NLO cross section is greater than that of the LO. Moreover the NLO QCD corrections can reduce the scale dependence of the LO cross section.

To summarize, the next-to-leading order QCD corrections to charged Higgs boson asso-

ciated production with top quark through $bg \rightarrow tH^-$ at the CERN Large Hadron Collider are calculated in the minimal supersymmetric standard model and two-Higgs-doublet model in the \overline{MS} scheme. The NLO QCD corrections can reduce the scale dependence of the LO cross section. The K-factor varies from ~ 1.4 to ~ 1.8 when charged Higgs mass and $\tan\beta$ are $180 \sim 1000$ GeV and $2 \sim 50$ respectively. We should note here that the results presented in this paper are for the process $bg \rightarrow tH^-$; they are the same for the charge conjugate process $\bar{b}g \rightarrow H^+\bar{t}$.

IV. ACKNOWLEDGEMENT

The author would like to thank Prof. W. Hollik, Prof. C.S. Li and Dr. J. Guasch for stimulating discussions. This work was supported in part by the Alexander von Humboldt Foundation and National Nature Science Foundation of China. Parts of the calculations have been performed on the QCM cluster at the University of Karlsruhe, supported by the DFG-Forschergruppe "Quantenfeldtheorie, Computeralgebra und Monte-Carlo-Simulation".

[1] For example to see, L. G. Jin, C. S. Li, R. J. Oakes and S. H. Zhu, Phys. Rev. D **62**, 053008 (2000) [arXiv:hep-ph/0003159], and references therein.

[2] W. Hollik and S. H. Zhu, hep-ph/0109103.

[3] D. P. Roy, Phys. Lett. B **459**, 607 (1999) [arXiv:hep-ph/9905542].

[4] K. Odagiri, Phys. Lett. B **452**, 327 (1999) [arXiv:hep-ph/9902303].

[5] F. Borzumati, J. L. Kneur and N. Polonsky, Phys. Rev. D **60**, 115011 (1999) [arXiv:hep-ph/9905443].

[6] L. G. Jin, C. S. Li, R. J. Oakes and S. H. Zhu, Eur. Phys. J. C **14**, 91 (2000) [arXiv:hep-ph/9907482].

[7] A. Belyaev, D. Garcia, J. Guasch and J. Sola, arXiv:hep-ph/0105053; C. S. Huang and S. H. Zhu, Phys. Rev. D **60**, 075012 (1999) [arXiv:hep-ph/9812201].

[8] J. Küblbeck, M. Böhm and A. Denner, Comput. Phys. Commun. **60**, 165 (1990); T. Hahn, hep-ph/9905354.

[9] R. Mertig, M. Böhm and A. Denner, Comput. Phys. Commun. **64**, 345 (1991).

[10] W. Beenakker, R. Hopker, M. Spira and P. M. Zerwas, Nucl. Phys. B **492**, 51 (1997) [arXiv:hep-ph/9610490].

[11] For example to see, B. W. Harris and J. F. Owens, hep-ph/0102128; S. H. Zhu, arXiv:hep-ph/0109269, to appear in Phys. Lett. B.

[12] S. Kawabata, Comput. Phys. Commun. 88, 309 (1995).

[13] H. L. Lai *et al.* [CTEQ Collaboration], Eur. Phys. J. C **12**, 375 (2000) [hep-ph/9903282].

[14] G. J. van Oldenborgh and J. A. Vermaseren, Z. Phys. C **46**, 425 (1990).

V. APPENDIX

In this appendix, we will give the non-vanishing form-factors in Eq. (13). For simplicity, we define abbreviation for $B_0^i (i = 1 - 7)$, $C_x^i (i = 1 - 8)$, $D_0^i (i = 1 - 3)$ as

$$\begin{aligned}
B_0^1 &= B_0(0, 0, m_t^2), \\
B_0^2 &= B_0(0, m_t^2, m_t^2), \\
B_0^3 &= B_0(m_{H^\pm}^2, 0, m_t^2), \\
B_0^4 &= B_0(m_t^2, 0, m_t^2), \\
B_0^5 &= B_0(s, 0, 0), \\
B_0^6 &= B_0(t, 0, m_t^2), \\
B_0^7 &= B_0(u, 0, m_t^2), \\
C_x^1 &= C_x(0, 0, s, 0, 0, 0), \\
C_x^2 &= C_x(0, m_{H^\pm}^2, t, m_t^2, m_t^2, 0), \\
C_x^3 &= C_x(m_{H^\pm}^2, 0, t, m_t^2, 0, 0), \\
C_x^4 &= C_x(m_{H^\pm}^2, 0, u, m_t^2, 0, 0), \\
C_x^5 &= C_x(m_{H^\pm}^2, m_t^2, s, 0, m_t^2, 0), \\
C_x^6 &= C_x(m_t^2, 0, t, m_t^2, 0, 0), \\
C_x^7 &= C_x(m_t^2, 0, u, 0, m_t^2, m_t^2), \\
C_x^8 &= C_x(m_t^2, 0, u, m_t^2, 0, 0), \\
D_0^1 &= D_0(m_{H^\pm}^2, 0, m_t^2, 0, t, u, 0, m_t^2, m_t^2, 0), \\
D_0^2 &= D_0(m_{H^\pm}^2, m_t^2, 0, 0, s, t, 0, m_t^2, 0, 0), \\
D_0^3 &= D_0(m_{H^\pm}^2, m_t^2, 0, 0, s, u, 0, m_t^2, 0, 0). \tag{38}
\end{aligned}$$

For diagram (e) in Fig. 2, we can write the form factor as

$$f_i = \frac{C_A}{2} \frac{g_s^3}{16\pi^2 s} g_i \tag{39}$$

$$\begin{aligned}
g_2 &= -2B_0^5 - s[C_0^1 + 3(C_1^1 + C_2^1)] + 4(-1 + 2\epsilon)C_{00}^1, \\
g_5 &= 2[B_0^5(1 + \epsilon) + s(C_0^1 + 2C_1^1 - 3C_2^1)]. \tag{40}
\end{aligned}$$

For diagram (f) in Fig. 2, we can write the form factor as

$$f_i = (C_F - C_A/2) \frac{g_s^3}{8\pi^2 s} g_i \quad (41)$$

$$\begin{aligned} g_2 &= -B_0^5 - (1 + \epsilon)s(C_0^1 + C_1^1 + C_2^1) + 2(1 - \epsilon)C_{00}^1, \\ g_5 &= (1 + \epsilon)B_0^5 + 2\epsilon sC_1^1 - 2(1 + \epsilon)sC_2^1. \end{aligned} \quad (42)$$

For diagram (g) in Fig. 2, we can write the form factor as

$$f_i = C_F \frac{g_s^3}{8\pi^2 s} g_i \quad (43)$$

$$\begin{aligned} g_1 &= m_t s(C_0^5(1 - \epsilon) + C_2^5 - \epsilon(C_1^5 + C_2^5)), \\ g_2 &= \frac{g_5}{2} = C_0^5(m_{H^\pm}^2 - 2m_t^2) - B_0^4 - B_0^5 - m_t^2(C_1^5 + C_2^5) + \epsilon(B_0^3 + sC_2^5). \end{aligned} \quad (44)$$

For diagram (h) in Fig. 2, we can write the form factor as

$$f_i = C_F \frac{g_s^3}{8\pi^2(m_t^2 - u)} g_i \quad (45)$$

$$\begin{aligned} g_1 &= m_t(-1 + \epsilon)(m_t^2 - u)(C_0^4 + C_1^4 + C_2^4), \\ g_2 &= \frac{g_3}{2} = -C_0^4[m_{H^\pm}^2 + (-2 + \epsilon)m_t^2 - \epsilon u] + B_0^7 \\ &\quad + m_t^2(C_1^4 + C_2^4) - \epsilon[B_0^3 + (m_t^2 - u)(C_1^4 + C_2^4)]. \end{aligned} \quad (46)$$

For diagram (i) in Fig. 2, we can write the form factor as

$$f_i = \frac{C_A}{2} \frac{g_s^3}{16\pi^2(m_t^2 - u)} g_i \quad (47)$$

$$\begin{aligned} g_1 &= 3m_t(m_t^2 - u)C_2^8, \\ g_2 &= 2B_0^4 + 2B_0^7 + (m_t^2 - u)(2C_0^8 + 3C_1^8) + 4(1 - \epsilon)C_{00}^8, \\ g_3 &= 2\{\epsilon - 1 + C_0^8(m_t^2 - u) - (1 + \epsilon)B_0^4 + 2B_0^7 + m_t^2[-5C_1^8 + 4C_2^8 + 2(1 - \epsilon)C_{11}^8] \\ &\quad + u[C_1^8 - 4C_2^8 - 2(1 - \epsilon)C_{11}^8]\}, \\ g_4 &= 4m_t[C_1^8 - 2C_2^8 - (1 - \epsilon)C_{11}^8]. \end{aligned} \quad (48)$$

For diagram (j) in Fig. 2, we can write the form factor as

$$f_i = (C_F - C_A/2) \frac{g_s^3}{8\pi^2(m_t^2 - u)} g_i \quad (49)$$

$$\begin{aligned} g_1 &= m_t(m_t^2 - u)[C_2^7 + \epsilon(C_0^7 + C_2^7)], \\ g_2 &= 2C_0^7 m_t^2 - (1 + \epsilon)B_0^2 + B_0^4 + B_0^7 + (1 + \epsilon)(m_t^2 - u)C_1^7 + 2(-1 + \epsilon)C_{00}^7, \\ g_3 &= -1 - B_0^4 + 2B_0^7 + 2uC_{22}^7 - 2m_t^2(2C_2^7 + C_{22}^7) \\ &\quad - \epsilon[-1 + B_0^4 - 2(m_t^2 - u)(C_2^7 + C_{22}^7)], \\ g_4 &= -2m_t[C_0^7 \epsilon + (-1 + 2\epsilon)C_2^7 + (-1 + \epsilon)C_{22}^7]. \end{aligned} \quad (50)$$

For diagram (k) in Fig. 2, we can write the form factor as

$$f_i = C_F \frac{g_s^3}{16\pi^2 s} g_i \quad (51)$$

$$g_2 = \frac{g_5}{2} = (1 - \epsilon)B_0^5. \quad (52)$$

For diagram (l) in Fig. 2, we can write the form factor as

$$f_i = C_F \frac{g_s^3}{16\pi^2(m_t^2 - u)^2 u} g_i \quad (53)$$

$$\begin{aligned} g_1 &= -m_t(m_t^2 - u) \left\{ (\epsilon - 1)m_t^2(B_0^1 - B_0^7) + u(\epsilon - 3)B_0^7 \right\}, \\ g_2 &= \frac{g_3}{2} = (-1 + \epsilon)m_t^4(B_0^1 - B_0^7) - (-1 + \epsilon)u^2 B_0^7 \\ &\quad + m_t^2 u \left\{ (1 - \epsilon)[B_0^1 - 2(1 + B_0^2)] + 2(-3 + \epsilon)B_0^7 \right\}. \end{aligned} \quad (54)$$

For diagram (m) in Fig. 2, we can write the form factor as

$$f_i = \frac{C_A}{2} \frac{g_s^3}{16\pi^2} g_i \quad (55)$$

$$\begin{aligned} g_1 &= -m_t[C_0^8 + C_1^8 + C_2^8 - 2(s - u + m_t^2)(D_0^3 + D_1 + D_2 + D_3) + 4D_{00}], \\ g_2 &= -2(C_0^4 + C_0^5) - 2D_0^3(m_t^2 - u) + C_1^1 + C_1^8 + 2(t + 2u)(D_2 + D_3) \\ &\quad - m_{H^\pm}^2(D_1 + 2D_2 + D_3) - m_t^2(D_1 + 4D_2 + 3D_3) + 4\epsilon D_{00}, \\ g_3 &= -2 \left\{ 2[C_0^4 - (1 + \epsilon)C_0^5 + C_0^8] - 2\epsilon(C_1^5 + C_2^5) + C_1^8 + C_2^8 + 2D_0^3[-m_{H^\pm}^2 + (1 - \epsilon)m_t^2 \right. \\ &\quad \left. + (1 + \epsilon)u] + 2[(3 - 2\epsilon)m_t^2 - t + 2u\epsilon](D_1 + D_2 + D_3) + 2[(1 - \epsilon)m_t^2 + u\epsilon](D_{11} \right. \end{aligned}$$

$$\begin{aligned}
& + 2D_{12} + 2D_{13} + D_{22} + 2D_{23} + D_{33})\} , \\
g_4 &= 4m_t \left\{ (D_2 + D_3 + D_{11} + 2D_{12} + D_{13} + D_{22} + D_{23}) - \epsilon[D_0^3 + D_{11} + D_{22} + D_{33} \right. \\
&\quad \left. + 2(D_1 + D_2 + D_3 + D_{12} + D_{13} + D_{23})] \right\} , \\
g_5 &= 4m_t \left\{ C_0^1 + 2\epsilon C_1^5 - C_1^1 + 2(u - m_t^2)D_1 + [m_{H^\pm}^2 - (7 - 2\epsilon)m_t^2 + 2(t + 2u) - 2u\epsilon]D_2 \right. \\
&\quad \left. + [-m_{H^\pm}^2 - m_t^2 + 2s]D_3 + [2(\epsilon - 1)m_t^2 - 2u\epsilon](D_{12} + D_{22} + D_{23}) \right\} , \\
g_6 &= -4m_t[D_0^3 + D_1 + (2 - \epsilon)D_2 + D_3 + D_{12} + D_{22}], \tag{56}
\end{aligned}$$

where the variable of the D-function is the same with D_0^3 .

For diagram (n) in Fig. 2, we can write the form factor as

$$f_i = (C_F - C_A/2) \frac{g_s^3}{8\pi^2} g_i \tag{57}$$

$$\begin{aligned}
g_1 &= -m_t \left\{ D_0^1[s + \epsilon(m_t^2 - u)] + s(D_2 + D_3) \right. \\
&\quad \left. - \epsilon[C_2^6 - m_t^2(D_1 + D_3) + u(D_2 + D_3)] - 2D_{00} \right\} , \\
g_2 &= -C_0^4 - C_0^7 + C_0^2(2 + \epsilon) + D_0^1[m_{H^\pm}^2 + \epsilon m_t^2 - (2 + \epsilon)u] + D_1[m_t^2(1 + \epsilon) \\
&\quad + s - u(1 + \epsilon)] + (D_2 + D_3)[\epsilon m_t^2 + s - u(1 + \epsilon)] - 2\epsilon D_{00}, \\
g_3 &= 2 \left\{ -C_0^4 - C_0^7 - (C_1^7 + C_2^7) - \epsilon(C_1^2 + C_2^6) + 2m_t^2 D_2 - t(D_2 + D_3) + m_t^2(2D_3 + D_{22} \right. \\
&\quad \left. + 2D_{23} + D_{33}) - \epsilon \left[C_2 + (m_t^2 - u)[D_2 + D_3 + D_{22} + 2D_{23} + D_{33}] \right] \right\} , \\
g_4 &= 2m_t \left\{ -D_2 - D_3 - D_{12} - D_{13} - D_{22} - 2D_{23} - D_{33} \right. \\
&\quad \left. + \epsilon[D_0^1 + 2D_2 + 2D_3 + D_{22} + 2D_{23} + D_{33}] \right\} , \\
g_5 &= -2 \left\{ C_0^6(-1 + \epsilon) + (4m_t^2 - t - 2u)D_2 - sD_3 + m_t^2(D_{22} + D_{23}) \right. \\
&\quad \left. + \epsilon[2C_1^6 - C_1^2 + C_2^6 - (m_t^2 - u)(D_3 + D_{22} + D_{23})] \right\} , \\
g_6 &= 2m_t[D_0 - (-3 + \epsilon)D_2 + D_{12} - (-1 + \epsilon)(D_{22} + D_{23})], \tag{58}
\end{aligned}$$

where the variable of the D-function is the same with D_0^1 .

For diagram (o) in Fig. 2, we can write the form factor as

$$f_i = (C_F - C_A/2) \frac{g_s^3}{8\pi^2} g_i \tag{59}$$

$$\begin{aligned}
g_1 &= -m_t[C_0^5 - \epsilon C_0^6 + D_0^2(1 + \epsilon)s - \epsilon(C_1^6 + C_2^6) + s(1 + \epsilon)(D_1 + D_2 + D_3) - 2D_{00}], \\
g_2 &= -C_0^1 - C_0^5 + C_0^3(2 + \epsilon) + D_0^2(-2m_t^2 + t) - m_t^2(D_1 + D_2)
\end{aligned}$$

$$\begin{aligned}
& + [s(1 + \epsilon) - u]D_3 - 2\epsilon D_{00}, \\
g_3 = & 2 \left\{ C_0^5(1 + \epsilon) - C_0^6\epsilon + D_0^2[2m_{H^\pm}^2 + m_t^2(4 - \epsilon) - s(2 - \epsilon) - 3t - u(2 - \epsilon)] \right. \\
& + \epsilon(C_1^3 + C_1^5 - C_1^6 + C_2^5 - C_2^6) + (D_1 + D_2 + D_3)[m_{H^\pm}^2(-3 + \epsilon) - m_t^2\epsilon + 3s + t(2 - \epsilon) \\
& \left. + u(3 + \epsilon)] + (D_{11} + 2D_{12} + 2D_{13} + D_{22} + 2D_{23} + D_{33})[m_t^2(1 - \epsilon) + \epsilon u] \right\}, \\
g_4 = & 2m_t \left\{ -D_3 - D_{13} - D_{23} - D_{33} + \epsilon(D_0 + 2D_1 + 2D_2 + 2D_3 + D_{11} \right. \\
& \left. + 2D_{12} + 2D_{13} + D_{22} + 2D_{23} + D_{33}) \right\}, \\
g_5 = & -2 \left\{ C_0^6 - D_0^2(m_{H^\pm}^2 - 2m_t^2) - C_1^1 + \epsilon(C_1^3 + C_2^5) + D_1[-t(1 + \epsilon) - 2u] + \right. \\
& (D_2 + D_3)[\epsilon m_{H^\pm}^2 - s(1 + \epsilon)] + D_3[-t(1 + \epsilon) - u] + (D_{11} + D_{12} + 2D_{13} + D_{23} + D_{33})u\epsilon \\
& \left. + m_t^2[5D_1 + D_2 + 4D_3 - (-1 + \epsilon)(D_{11} + D_{12} + 2D_{13} + D_{23} + D_{33})] \right\}, \\
g_6 = & 2m_t \left\{ D_0^2 - (-2 + \epsilon)(D_1 + D_3) + D_{13} + D_{33} - \epsilon(D_{11} + D_{12} + 2D_{13} + D_{23} + D_{33}) \right\}, \quad (60)
\end{aligned}$$

where the variable of the D-function is the same with D_0^2 .

By decomposition, the loop integrations in above form-factors can be calculated by the limit number of scalar integrates B_0 , C_0 and D_0 . The scalar integrates C_0 and D_0 are UV finite, however some of them contain infrared and collinear divergences. Because the finite scalars integration could be calculated by numerical method [14], only the divergent ones are presented explicitly in this paper. It should be noted that only real part of the integration, which is relevant to our results, is given.

D_0 and C_0 scalar integrates could be generally written as

$$\begin{aligned}
D_0 &= \frac{(4\pi\mu^2)^\epsilon\Gamma(2 + \epsilon)}{1 + \epsilon} \left(\frac{d_2}{\epsilon^2} + \frac{d_1}{\epsilon} + d_0 \right), \\
C_0 &= -(4\pi\mu^2)^\epsilon\Gamma(1 + \epsilon) \left(\frac{c_2}{\epsilon^2} + \frac{c_1}{\epsilon} + c_0 \right).
\end{aligned} \quad (61)$$

The coefficients d_2 , d_1 and d_0 of D_0^1 are

$$d_2 = \frac{1}{2(-t + m_t^2)(-u + m_t^2)}, \quad (62)$$

$$d_1 = \frac{\log(m_t) - \log(-t + m_t^2) - \log(-u + m_t^2) + \log(-m_H^2 + m_t^2)}{(-t + m_t^2)(-u + m_t^2)}, \quad (63)$$

$$d_0 = \frac{1}{2(-t + m_t^2)(-u + m_t^2)} \left\{ 6\log^2(m_t) + 8\log(m_{H^\pm})\log(m_t) - 4\log(m_t^2 - t)\log(m_t) \right. \\$$

$$\begin{aligned}
& -4 \log(t) \log(m_t) - 4 \log(m_t^2 - t) \log(m_t) - 4 \log(u) \log(m_t) + 4 \log|m_{H^\pm}^2 - m_t^2| \log(m_t) \\
& + \log^2(m_t^2 - t) + \log^2(m_t^2 - u) - \log^2|m_{H^\pm}^2 - m_t^2| - 4 \log^2(m_t^2 - t) \log^2(m_{H^\pm}^2 - t) \\
& + 2 \log^2(m_t^2 - t) \log(t) + 8 \log(m_t^2 - t) \log(m_t^2 - u) - 4 \log^2(m_t^2 - u) \log^2(m_{H^\pm}^2 - u) \\
& + 2 \log^2(m_t^2 - u) \log(u) - 4 \log(m_{H^\pm}) \log|m_{H^\pm}^2 - m_t^2| + 4 \log(m_{H^\pm}^2 - t) \log|m_{H^\pm}^2 - m_t^2| \\
& - 4 \log(m_t^2 - t) \log|m_{H^\pm}^2 - m_t^2| + 4 \log(m_{H^\pm}^2 - u) \log|m_{H^\pm}^2 - m_t^2| \\
& - 4 \log(m_t^2 - u) \log|m_{H^\pm}^2 - m_t^2| + 2li_2\left(\frac{tu - m_{H^\pm}^2 m_t^2}{(m_{H^\pm}^2 - t)(m_{H^\pm}^2 - u)}\right) + 2li_2\left(\frac{m_{H^\pm}^2 m_t^2 - tu}{m_t^2 (m_{H^\pm}^2 - u)}\right) \\
& + 2li_2\left(\frac{m_{H^\pm}^2}{m_{H^\pm}^2 - m_t^2}\right) - 2li_2\left(\frac{s}{-t + m_t^2}\right) - 2li_2\left(\frac{t}{t - m_t^2}\right) - 2li_2\left(\frac{m_{H^\pm}^2 - t}{m_t^2 - u} + 1\right) \\
& + 2li_2\left(\frac{(m_{H^\pm}^2 - m_t^2)s}{(m_t^2 - t)(u - m_t^2)}\right) - 2li_2\left(\frac{u}{u - m_t^2}\right) + 2li_2\left(\frac{m_{H^\pm}^2 m_t^2 - tu}{m_t^2 (m_{H^\pm}^2 - t)}\right) \\
& - 2li_2\left(\frac{(m_{H^\pm}^2 - m_t^2)(m_{H^\pm}^2 m_t^2 - tu)}{m_t^2 (m_{H^\pm}^2 - u)(m_{H^\pm}^2 - t)}\right) - 2li_2\left(\frac{m_{H^\pm}^2 m_t^2 - tu}{(m_{H^\pm}^2 - t)(m_t^2 - t)}\right) \\
& + 2li_2\left(\frac{tu - m_{H^\pm}^2 m_t^2}{(m_t^2 - t)(m_t^2 - u)}\right) - 2li_2\left(\frac{m_{H^\pm}^2 m_t^2 - tu}{(m_{H^\pm}^2 - u)(m_t^2 - u)}\right) + \pi^2 \theta(m_{H^\pm} - m_t) \Big\}. \quad (64)
\end{aligned}$$

The coefficients d_2 , d_1 and d_0 of D_0^2 are

$$d_2 = -\frac{3}{2s(-t + m_t^2)}, \quad (65)$$

$$d_1 = \frac{1}{s(-t + m_t^2)} \left\{ 4 \log(m_t^2 - t) - \log(m_{H^\pm}^2 - t) + 2 \log(s) - \log(m_t^2) - \log(m_{H^\pm}^2 - m_t^2) \right\}, \quad (66)$$

$$\begin{aligned}
d_0 = & \frac{1}{2s(-t + m_t^2)} \left\{ \pi^2 \left[\frac{4}{3} - \theta(m_{H^\pm} - m_t) \right] + 2 \log^2(m_t) + 4 \log(m_t) [\log(s) + \log(m_{H^\pm}^2 - t) \right. \\
& - 2 \log|m_{H^\pm}^2 - m_t^2|] + 3 \log^2|m_{H^\pm}^2 - m_t^2| - \log(m_t^2 - t) [4 \log(s) - 2 \log(m_{H^\pm}^2 - t) \\
& + 3 \log(m_t^2 - t)] + 4 \log|m_{H^\pm}^2 - m_t^2| [\log(m_t^2 - t) - \log(m_{H^\pm}^2 - t)] + 2li_2\left(\frac{m_t^2}{m_t^2 - m_{H^\pm}^2}\right) \\
& \left. - 2li_2\left(\frac{t}{m_t^2}\right) + 2li_2\left(\frac{(m_{H^\pm}^2 - m_t^2)t}{m_t^2(m_{H^\pm}^2 - t)}\right) - 2li_2\left(\frac{t}{t - m_{H^\pm}^2}\right) - 2li_2\left(\frac{m_{H^\pm}^2 - m_t^2}{t - m_t^2}\right) \right\}. \quad (67)
\end{aligned}$$

The coefficients c_2 , c_1 and c_0 of C_0^1 are

$$c_2 = -\frac{1}{s}, \quad (68)$$

$$c_1 = \frac{\log(s)}{s}, \quad (69)$$

$$c_0 = \frac{1}{6s} [4\pi^2 - 3\log^2(s)]. \quad (70)$$

The coefficients c_1 and c_0 of C_0^3 are

$$c_1 = \frac{1}{m_{H^\pm}^2 - t} \log \left(\frac{m_t^2 - m_{H^\pm}^2}{m_t^2 - t} \right), \quad (71)$$

$$c_0 = \frac{1}{m_{H^\pm}^2 - t} \left\{ -\frac{1}{2} \log^2 |m_{H^\pm}^2 - m_t^2| + \frac{1}{2} \log^2(m_t^2 - t) + \log \left(1 - \frac{m_{H^\pm}^2}{m_t^2} \right) \log \left(\frac{m_{H^\pm}^2}{m_{H^\pm}^2 - m_t^2} \right) \right. \\ \left. - \log \left(\frac{t}{t - m_t^2} \right) \log \left(1 - \frac{t}{m_t^2} \right) - li_2 \left(\frac{m_t^2}{m_t^2 - m_{H^\pm}^2} \right) + li_2 \left(\frac{m_t^2}{m_t^2 - t} \right) \right\}. \quad (72)$$

The coefficients c_2, c_1 and c_0 of C_0^6 are

$$c_2 = \frac{1}{2(m_t^2 - t)}, \quad (73)$$

$$c_1 = \frac{1}{2(m_t^2 - t)} \left\{ \log(m_t^2) - 2\log(m_t^2 - t) \right\}, \quad (74)$$

$$c_0 = \frac{1}{4(m_t^2 - t)} \left\{ -\frac{2}{3}\pi^2 - \log(m_t^2) + 2\log^2(m_t^2 - t) - 4\log \left(\frac{t}{t - m_t^2} \right) \log \left(\frac{m_t^2 - t}{m_t^2} \right) \right. \\ \left. + 4li_2 \left(\frac{m_t^2}{m_t^2 - t} \right) \right\}. \quad (75)$$

C_0^4, C_0^8 and D_0^3 can be obtained from C_0^3, C_0^6 and D_0^2 by replacing t with u .

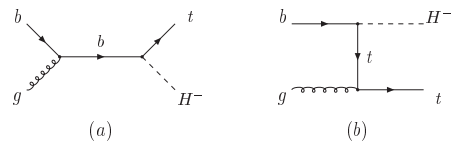


FIG. 1. Feynman diagrams at LO for $bg \rightarrow tH^-$.

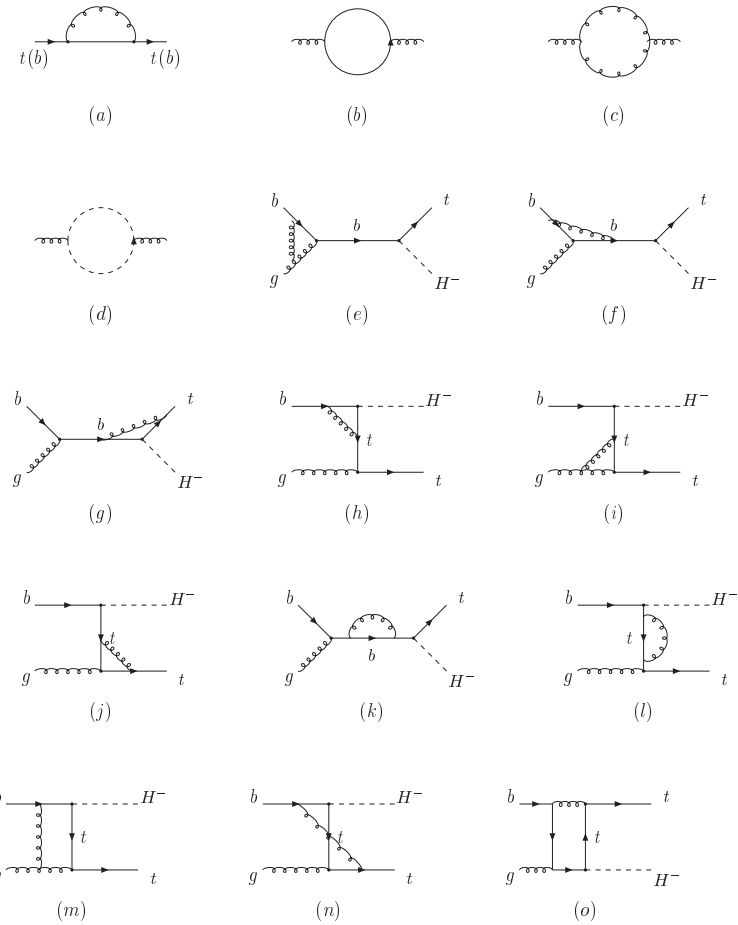


FIG. 2. Feynman diagrams of the virtual correction for the process $bg \rightarrow tH^-$.

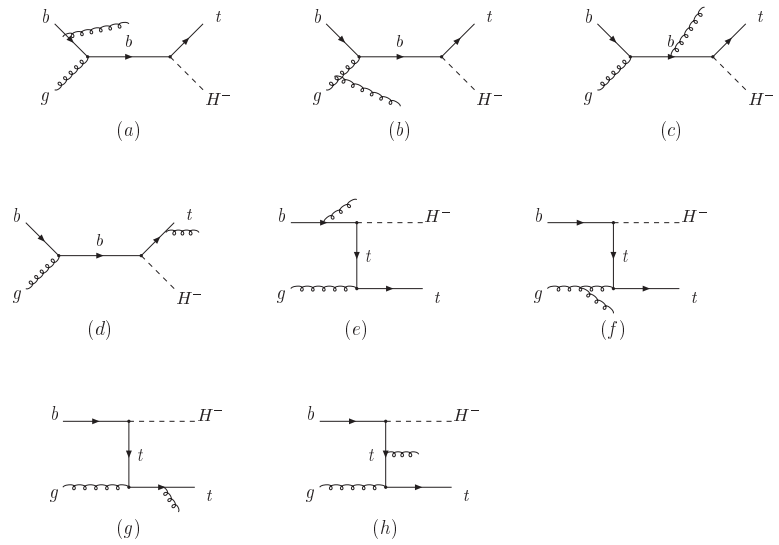


FIG. 3. Feynman diagrams of gluon-radiation process of $bg \rightarrow tH^- g$.

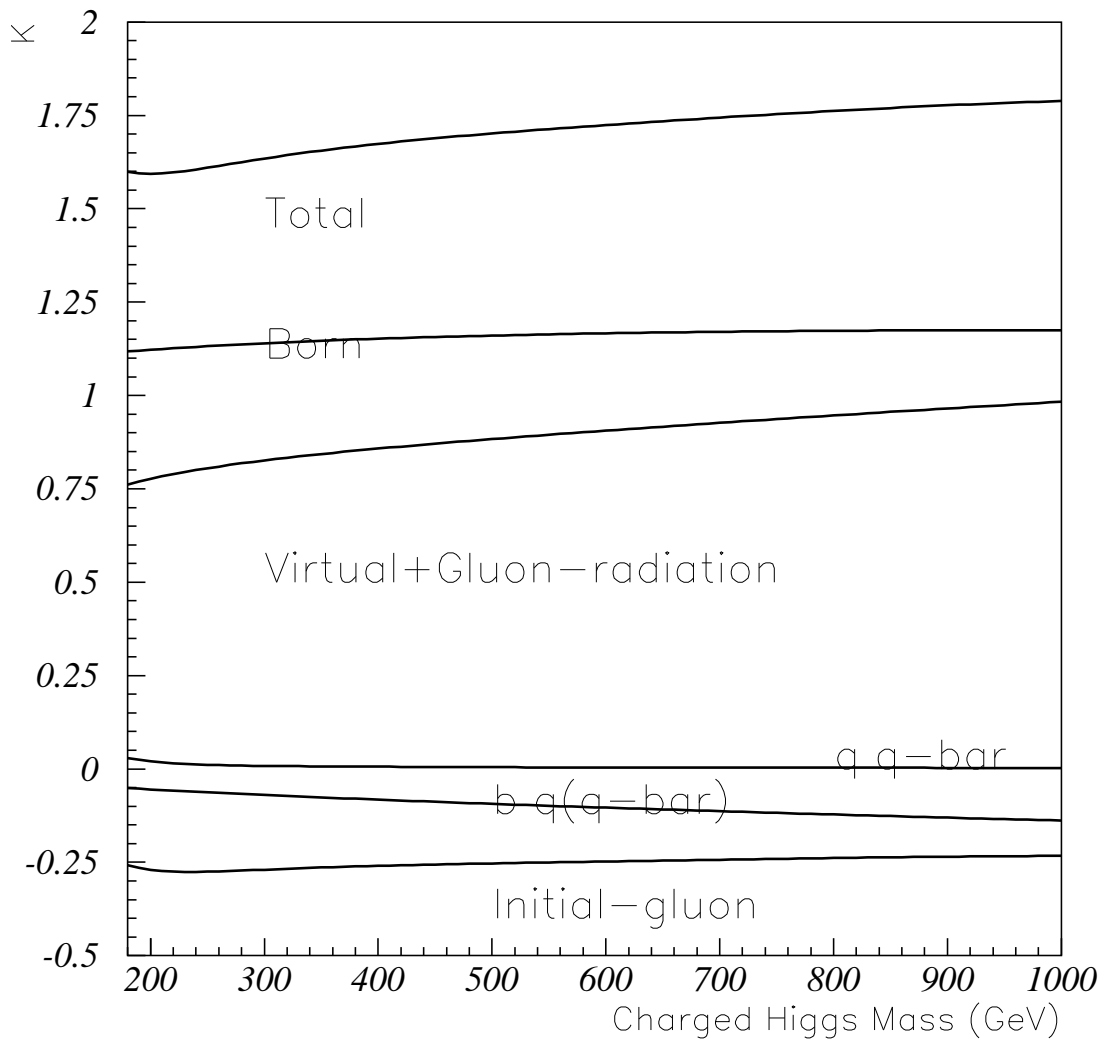


FIG. 4. K-factor (defined in text) versus m_{H^\pm} with $\tan\beta = 50$.

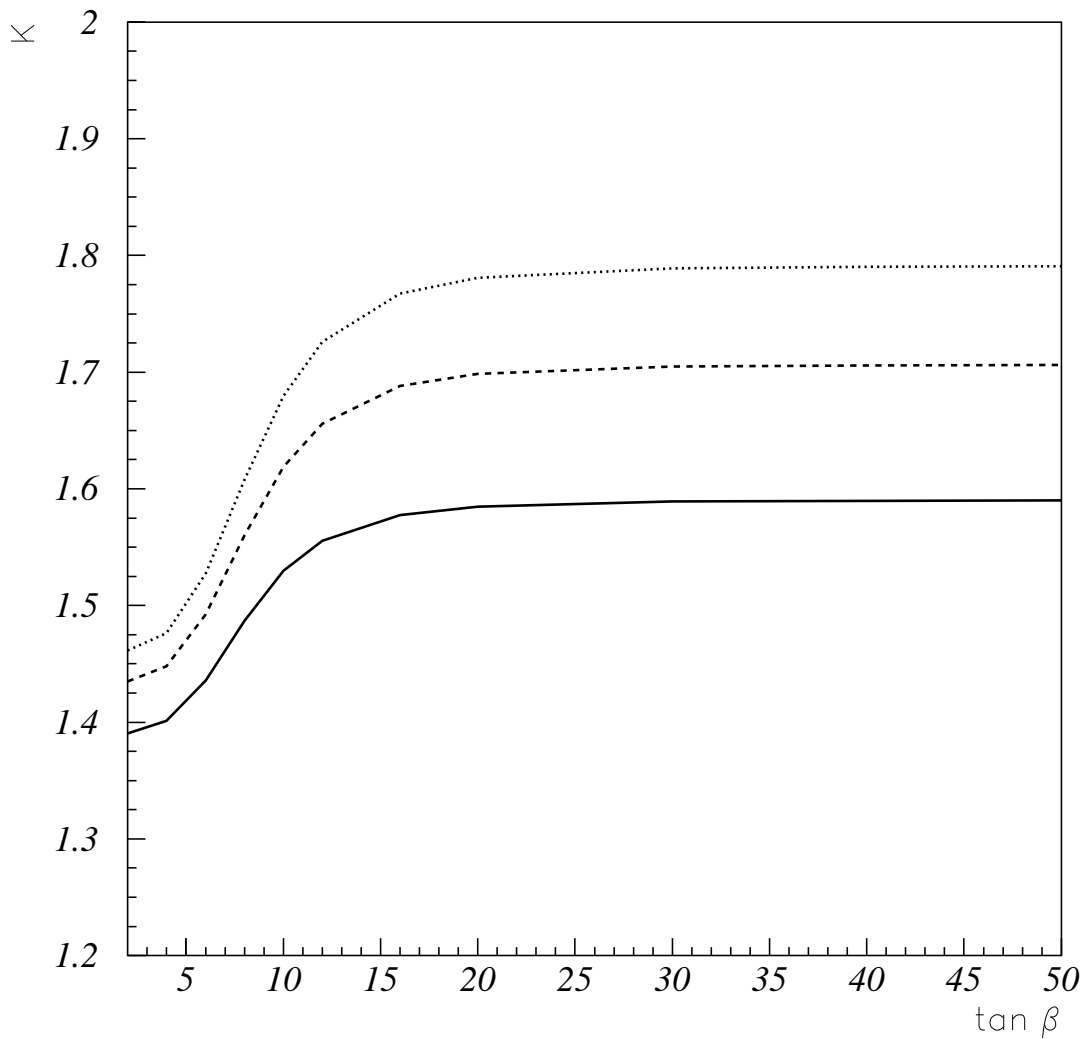


FIG. 5. K-factor versus $\tan \beta$. The solid, dashed and dotted lines represent $m_{H^\pm} = 200, 500$ and 1000 GeV, respectively.

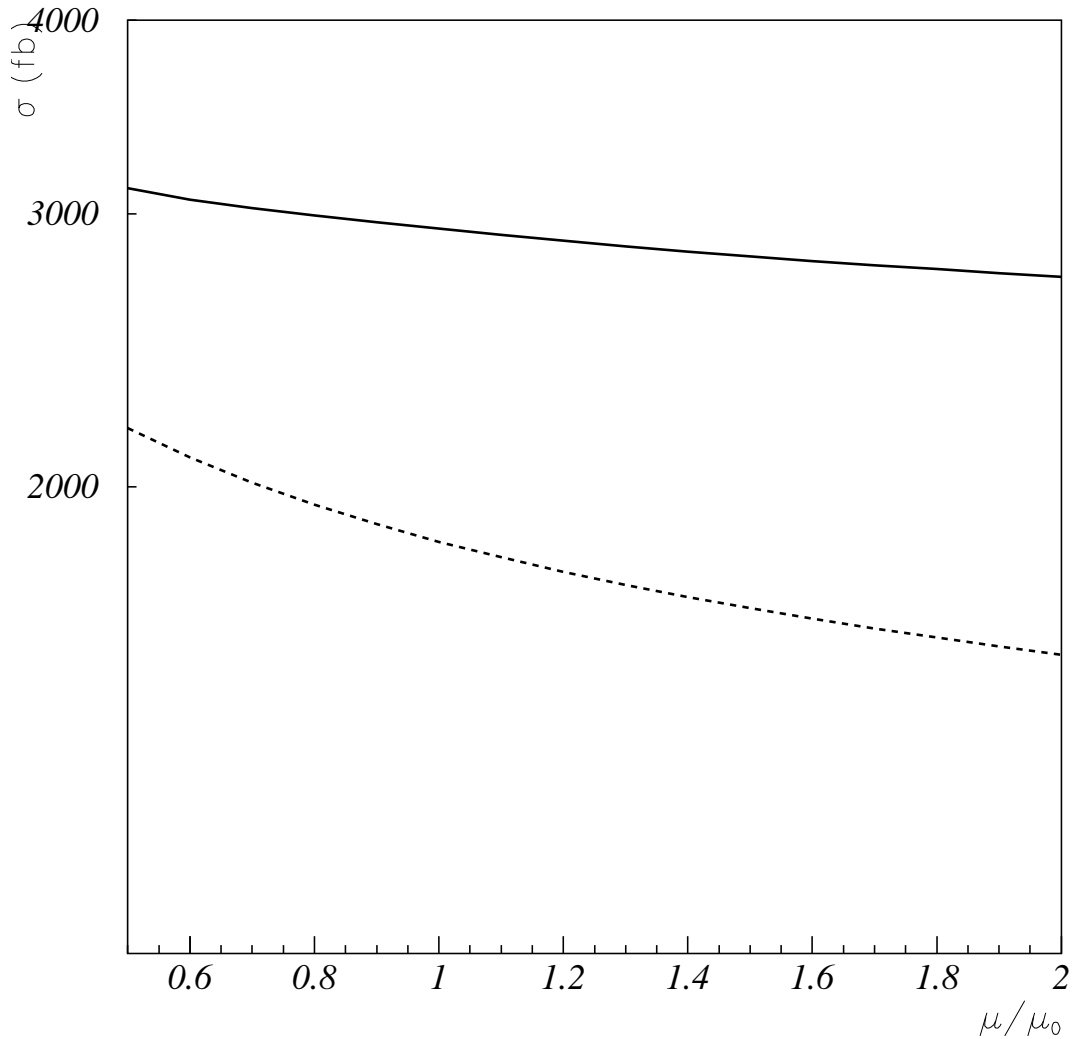


FIG. 6. Total cross sections for the process $PP \rightarrow tH^-X$ as a function of μ/μ_0 , where $\mu_0 = m_{H^\pm} + m_t$, $m_{H^\pm} = 200$ GeV and $\tan \beta = 50$. Solid and dashed lines represent results at NLO and LO.